Rochester Institute of Technology
RIT Digital Institutional Repository

Presentations and other scholarship | Faculty & Staff Scholarship

5-5-1995

Experimental verification of a novel system ID technique called PLID using a flexible 3-D structure

Phillip Vallone
Eastman Kodak Co.

Mark A. Hopkins
Rochester Institute of Technology

Follow this and additional works at: https://repository.rit.edu/other

Recommended Citation

Phillip Vallone, Mark A. Hopkins, "Experimental verification of a novel system ID technique called pseudolinear identification (PLID) using a flexible 3D structure", Proc. SPIE 2442, Smart Structures and Materials 1995: Mathematics and Control in Smart Structures, (5 May 1995); doi: 10.1117/12.208845; https://doi.org/10.1117/12.208845

This Conference Paper is brought to you for free and open access by the RIT Libraries. For more information, please contact repository@rit.edu.

Copyright 1995 Society of Photo-Optical Instrumentation Engineers.

This paper was published by SPIE and is made available as an
electronic reprint (preprint) with permission of SPIE. One print or electronic copy may be made for personal use only. Systematic or multiple reproduction, distribution to multiple locations via electronic or other means, duplication of any material in this paper for a fee or for commercial purposes, or modification of the content of the paper are prohibited.

Experimental verification of a novel system ID technique called PLID using a flexible 3-D structure

Phillip Vallone and Mark A. Hopkins

ABSTRACT

Presented below is a summary of the results obtained to date on the verification of a novel state space model identification technique called PLID (Pseudo Linear IDentification), given in Hopkins *et al.*[1] This technique has several unique features that include: (1) optimal *joint* parameter and state estimation (that gives rise to its nonlinearities); (2) provisions for sensor, actuator, and state noise; (3) and it converges almost surely to the true plant parameters provided that the plant is linear, completely controllable/observable, strictly proper, time invariant, and all noise sources are zero mean white gaussian (ZMWG).

Experiments carried out on a flexible, modally dense 3-D truss structure standing 4 feet tall have shown PLID to be a robust technique capable of managing significant deviations from the assumptions made to prove strict optimality. Using the 3 actuators and 3 sensors attached to the structure, models varying in size from 24 to 64 states have been used to approximate this infinite dimensional testbed in the frequency range between 50 to 500 Hz. Sensor signals with RMS levels of approximately 2 volts have been predicted by PLID to within 0.01 volts RMS.

Keywords: system identification, MIMO, control system, piezo-ceramic actuator, accelerometer, LQG, large structures

1.0 INTRODUCTION

The need for system ID is twofold. First, in order to facilitate the design of a high-performance model based controller, one must have a high fidelity math model upon which to base a design. For complex structures, the math modeling tools most often used (e.g., finite element analysis) are not adequate. A more accurate model can be obtained using experimentally determined plant parameters. Secondly, any analysis of the plant, not necessarily related to control system design, can be performed using a model generated from input/output data. Such analyses may include health monitoring, performance predictions, and on-line component testing, to name a few.

PLID is fully mathematically described in Hopkins *et al.* and will not be repeated below in great detail. Herein, we wish to describe the testbed that has been used to validate PLID and the experimental results obtained to date. This testbed has been fabricated for the purposes of showing PLID's general applicability, even to infinite dimensional (which drives the need for model order reduction), modally dense systems such as a symmetrical 3-D truss structure.

As with most flexible structures, the testbed is modally dense, lightly damped, and, because of its construction, slowly time varying and weakly nonlinear. PLID is shown to be able to perform what is essentially model order reduction. Further, we demonstrate its robustness to deviations from the ideal time-invariant, linear, finite-dimensional requirements needed to strictly prove PLID's optimality. Both multi-input multi-output (MIMO) and single-input-multi-output (SIMO) models were generated for the testbed. In general, PLID was able to produce a states space model that could mimic the testbed's sensor output (accelerometers) to within the sensor's noise level of approximately 10 mV. Excited with the actuators, the sensor could be driven to output 2 V RMS signals, yielding a "signal to prediction error" ratio of 46 dB.

2.0 BACKGROUND INFORMATION

2.1 Motivation

With "smart structures" covering an ever expanding range of physical devices from large space structures to miniature disk drive read arms, a huge amount of research has gone into the modeling of these systems. And although the underlying physics of flexible mechanical systems are well understood, often the system of interest is simply too complex to model accurately enough to use with high performance MIMO feedback controllers. Detailed finite element math models are difficult to generate and do not include noise sources. Further, exact dimensions, densities, and moduli of

elasticity of the various materials that compose the structure are virtually impossible to come by. Thus the attraction of model identification techniques.

Particularly for controls engineers, a state space input/output characterization of the system is often the end goal or result of a modeling exercise. The effort expended to obtain this model can be considerable, if not prohibitive. System ID techniques exist that can directly provide such a state space model using the same actuator-sensor suite to be used for control. PLID is one such technique.

2.2 Model structure

As mentioned, PLID is a state space model identifier. When provided with an estimate of the sensor, actuator, and state noise covariances, and input/output data of sufficient spectral richness (more on this later), PLID will generate an *A* and a *B* matrix, with the *C* matrix known *a priori*. Given the nearly linear, relatively time-invariant nature of many flexible structures, PLID should be able to estimate these matrices as long as one attempts to limit the observability and/or controllability of high-frequency modes. That is, since every mechanical system can be described by an infinite dimensional state space model, an attempt must be made to limit the bandwidth of interest to some reasonable bound, lest the model become completely unwieldy.

By the assumption of complete observability and controllability (required for system ID), we can cast the system into MIMO observable canonic form, with additive ZMWG noise v_k and w_k corrupting the input $u_k \in \Re^m$ and output $y_k \in \Re^p$, respectively. State noise Ξ_x is also allowed. One can see from the below formulation, the *C* matrix is known *a priori*, the *B* matrix is completely unknown, and the *A* matrix has exactly p unknown columns.

Thus the number of parameters to be identified is equal to pxn in the *A* matrix (referred to as *A* parameters), mxn in the *B* matrix (*B* parameters), and n states, giving a total of (p+m+1)n unknowns. We are computing a minimum-mean-square-error recursive prediction, conditioned on the past inputs and sensor outputs.

Since the cost functional for PLID is essentially the same as that used by a Kalman filter (KF), the form of the PLID algorithm is very similar to Kalman's algorithm (see Brown *et al.* for information on the KF).[2] Like the KF, PLID also has 3 essential equations: (1) the "gain computation", (2) the "state propagation", and (3) the "error covariance propagation" equation. Only for PLID the "states" are now both states and system parameters that make up the *A* and *B*

$$\mathbf{x}_{k+1} = \begin{bmatrix} x_{1,1} \\ \vdots \\ x_{1,n_1} \\ \cdots\cdots \\ x_{p,1} \\ \vdots \\ x_{p,n_p} \end{bmatrix}_{k+1} = \left[\begin{array}{ccccc|c|ccccc} 0 & \cdots & 0 & a^0_{1,1} & & & 0 & \cdots & 0 & a^0_{p,1} \\ 1 & & 0 & a^1_{1,1} & & & 0 & \cdots & 0 & a^1_{p,1} \\ & \ddots & \vdots & \vdots & & & \vdots & & \vdots & \vdots \\ 0 & \cdots & 1 & a^{n_1-1}_{1,1} & & & 0 & \cdots & 0 & a^{n_1-1}_{p,1} \\ \hline & & & & \ddots & & & & & \\ \hline 0 & \cdots & 0 & a^0_{1,p} & & & 0 & \cdots & 0 & a^0_{p,p} \\ 0 & \cdots & 0 & a^1_{1,p} & & & 1 & & 0 & a^1_{p,p} \\ \vdots & & \vdots & \vdots & & & & \ddots & \vdots & \vdots \\ 0 & \cdots & 0 & a^{n_p-1}_{1,p} & & & 0 & \cdots & 1 & a^{n_p-1}_{p,p} \end{array}\right] \begin{bmatrix} x_{1,1} \\ \vdots \\ x_{1,n_1} \\ \cdots\cdots \\ x_{p,1} \\ \vdots \\ x_{p,n_p} \end{bmatrix}_k + \left[\begin{array}{ccc} b^0_{1,1} & \cdots & b^0_{m,1} \\ \vdots & & \vdots \\ b^{n_1-1}_{1,1} & \cdots & b^{n_1-1}_{m,1} \\ \hline \vdots & & \vdots \\ \hline b^0_{1,p} & \cdots & b^0_{m,p} \\ \vdots & & \vdots \\ b^{n_p-1}_{1,p} & \cdots & b^{n_p-1}_{m,p} \end{array}\right] \begin{bmatrix} u_1 + v_1 \\ \vdots \\ u_m + v_m \end{bmatrix}_k + \begin{bmatrix} \varepsilon_{1,1} \\ \vdots \\ \varepsilon_{1,n_1} \\ \cdots\cdots \\ \varepsilon_{p,1} \\ \vdots \\ \varepsilon_{p,n_p} \end{bmatrix}_k \quad (1)$$

$$\equiv \mathbf{A}_k \mathbf{x}_k + \mathbf{B}_k(\mathbf{u}_k + \mathbf{v}_k) + \Xi_k$$

$$\mathbf{z}_k \equiv \begin{bmatrix} z_1 \\ \vdots \\ z_p \end{bmatrix}_k = \left[\begin{array}{ccccc|c|ccc} 0 & \cdots & 0 & 1 & & & 0 & & 0 & 0 \\ \hline & & & & \ddots & & & & & \\ \hline 0 & \cdots & 0 & 0 & & & 0 & \cdots & 0 & 1 \end{array}\right] \begin{bmatrix} x_{1,1} \\ \vdots \\ x_{1,n_1} \\ \cdots\cdots \\ x_{p,1} \\ \vdots \\ x_{p,n_p} \end{bmatrix}_k + \begin{bmatrix} w_1 \\ \vdots \\ w_m \end{bmatrix}_k \equiv \mathbf{C}\mathbf{x}_k + \mathbf{w}_k \quad (2)$$

matrices. It is the joint state and parameter estimation that gives rise to the nonlinear terms in the gain and covariance equations. As Hopkins *et al.* mention, at first glance the PLID equations look very much like those governing the KF, which is linear. However, upon closer inspection, one sees that the PLID equations contain cross-multiples of the state estimates. Hence the name "pseudo-linear".

2.3 Overview of PLID

The derivation of PLID involves forming an extended state vector by appending the *A* parameters and the *B* parameters to the states. Doing this forces the original state equations (Eq. 1 and 2) to be completely rewritten into an "extended Salut form", after the work of Salut *et al.*[3] Once in this form, the derivation parallels the KF.

The extended state vector has the form shown in Eq. 3. From this state vector s_k, we can create the extended state equations, or the *implicit model* $\overline{S}$, as Hopkins *et al.* refer to it. The various matrices that appear in Eq. 3 are

$$s_k \equiv \begin{bmatrix} x_k \\ \hdashline \Theta_A \\ \hdashline \Theta_B \end{bmatrix} \equiv \begin{bmatrix} x_k \\ \hdashline \Theta^1{}_A \\ \vdots \\ \Theta^p{}_A \\ \hdashline \Theta^1{}_B \\ \vdots \\ \Theta^m{}_B \end{bmatrix} \tag{3}$$

$$\text{where } \Theta^i{}_A \equiv \left[a_{i,1}^0 \quad \cdots \quad a_{i,1}^{n_1-1} \;\middle|\; \cdots \;\middle|\; a_{i,p}^0 \quad \cdots \quad a_{i,p}^{n_p-1} \right]^T$$

$$\text{and} \quad \Theta^i{}_B \equiv \left[b_{i,1}^0 \quad \cdots \quad b_{i,1}^{n_1-1} \;\middle|\; \cdots \;\middle|\; b_{i,p}^0 \quad \cdots \quad b_{i,p}^{n_p-1} \right]^T$$

elaborated. The "A parameters", denoted by $\Theta^i{}_A$, are the ith column of the *A* matrix, which has p such columns, as noted in Eq. 1; similarly, the "B parameters", $\Theta^i{}_B$, hold the ith column of the m full columns in the *B* matrix. The variables n_1, n_2, ... , n_p are called the observability indices, which refer to the number of states that are associated with a particular output; e.g., the first n_1 states are associated with $y_1(k)$ and the next n_2 states are associated with $y_2(k)$, etc...

Next, new state space equations are built around the extended state vector s_k. We will skip the details of how these equations are arrived at; these details are found in Hopkins *et al.*

$$\text{Implicit Model: } \overline{S} \begin{cases} s_{k+1} = \mathbf{F}_k s_k + \mathbf{G}\eta_k \\ z_k = \mathbf{H} s_k + w_k \end{cases} \tag{4}$$

where

$$\mathbf{F}_k = \left[\begin{array}{cccc|c} \mathbf{J}_{n_1} & \mathbf{0} & \cdots & \mathbf{0} & \\ \mathbf{0} & \mathbf{J}_{n_2} & & \vdots & \\ \vdots & & \ddots & \mathbf{0} & z_1(k)\mathbf{I}_n \quad \cdots \quad z_p(k)\mathbf{I}_n \quad u_1(k)\mathbf{I}_n \quad \cdots \quad u_m(k)\mathbf{I}_n \\ \mathbf{0} & \cdots & \mathbf{0} & \mathbf{J}_{n_p} & \\ \hline \multicolumn{4}{c|}{\mathbf{0}_{(m+p)nxn}} & \mathbf{I}_{(m+p)n} \end{array} \right], \tag{4a}$$

$$\mathbf{G} = \left[\begin{array}{c|c|c|c|c|c|c|c} -\Theta^1{}_A & \cdots & -\Theta^p{}_A & \Theta^1{}_B & \cdots & \Theta^p{}_B & \mathbf{I}_n & \mathbf{0} \\ \hline \mathbf{0} & \cdots & \mathbf{0} & \mathbf{0} & \cdots & \mathbf{0} & \mathbf{0} & \mathbf{I}_{(m+p)n} \end{array} \right] \tag{4b}$$

$$n_k = \left[w^T{}_k \quad v^T{}_k \quad \Xi^T{}_k \quad 0^T{}_{(m+p)n} \right]^T , \tag{4c}$$

and

$$\mathbf{H} = \left[\begin{array}{ccc|ccc|c|ccc|c} 0 & \cdots & 0\,1 & 0 & \cdots & 0\,0 & \cdots & 0 & \cdots & 0\,0 & \\ 0 & \cdots & 0\,0 & 0 & \cdots & 0\,1 & & & \vdots & & \mathbf{0}_{p\times(m+p)n} \\ & \vdots & & & & & \ddots & 0 & \cdots & 0\,0 & \\ 0 & \cdots & 0\,0 & 0 & \cdots & 0\,0 & & 0 & \cdots & 0\,1 & \end{array}\right] . \tag{4d}$$

Notice the upper left matrix partition of Eq. 4a. This submatrix is further subdivided into p, n_ixn_i, lower Jordan blocks ($\mathbf{J}_{n_i}$) of zero eigenvalues. Also note that the lower right partition of F_k is an identity matrix of dimension equal to the number of A and B parameters. That is, $s_j(k+1) = s_j(k)$ for j>n, which agrees with the requirement that plant parameters be time invariant.

Acting as an input to the implicit model is η_k. This is a vector of noise vectors, where all elements corresponding to plant parameters are zero, which also agrees with the time invariant requirement. Although plant parameter time invariance is needed to prove PLID's optimality, it is useful to add very small amounts of noise to the parameters to increase the algorithm's stability when implemented using finite precision math and without using a square root algorithm. If PLID is implemented using a square root formulation such as given by Bierman[4], then parameter noise does not appear to be needed; however, such robust algorithms do require significantly more computations. One may wish to directly implement PLID, as is, for small problems not likely to exhibit stability problems; e.g., when the number of states is ≤ 12. Notice that the output equation in Eq. 4 is nearly the same as in Eq. 2 of the explicit model. This is a direct result of formulating the system in the MIMO observable canonic form (see for example Kailath pp. 424 to 437).[5]

All noise sources encompassed in η_k are assumed to have known covariances and crosscovariances for all time k; that is:

$$\mathbf{Q}^o{}_k \equiv E[n_k n_k{}^T] \equiv \left[\begin{array}{ccc|c} \mathbf{R}_k & \mathbf{S}_k^{w\nu} & \mathbf{S}_k^{w\Xi} & \\ \mathbf{S}_k^{\nu w} & \mathbf{Q}_k & \mathbf{S}_k^{\nu\Xi} & \mathbf{0} \\ \mathbf{S}_k^{\Xi w} & \mathbf{S}_k^{\Xi\nu} & \Sigma_k & \\ \hline & \mathbf{0} & & \mathbf{0}_{(m+p)n\times(m+p)n} \end{array}\right] . \tag{5}$$

$$\text{where covariances:} \quad E[v_k v_k{}^T] \equiv \mathbf{Q}_k,\ E[w_k w_k{}^T] \equiv \mathbf{R}_k,\ \text{and}\ E[\Xi_k \Xi_k{}^T] \equiv \Sigma_k, \tag{6}$$

$$\text{and cross-covariances:} \quad \mathbf{S}_k^{\alpha\beta} \equiv E[\alpha_k \beta_k{}^T],$$

are as denoted. Further, Hopkins *et al.* goes on to denote the input/output cross-covariances of the implicit model by:

$$S_k \equiv E[n_k w_k{}^T] \equiv \left[\begin{array}{c} \mathbf{R}_k \\ \mathbf{S}_k^{\nu w} \\ \mathbf{S}_k^{\Xi w} \\ \mathbf{0}_{(m+p)n\times p} \end{array}\right] . \tag{7}$$

Finally, the cost functional is defined, which is the same functional used by the KF, as the linear conditional minimum-mean-square-error (MMSE) recursive prediction $\hat{s}_{k+1|k}$ of the extended state vector s_{k+1}. An optimal gain matrix ($\mathbf{K}_k$) will be arrived at in the same way as in the KF. We will not reproduce the derivation here, instead we provide the key results below:

$$\text{Optimal Gain: } \mathbf{K}_k = \left[\mathbf{F}_k \mathbf{P}_{k|k-1}\mathbf{H}^T + E_{\psi_k}[\mathbf{G}]\mathbf{S}_k\right]^T \left[\mathbf{H}\mathbf{P}_{k|k-1}\mathbf{H}^T + \mathbf{R}_k\right]^{-1} \tag{8}$$

$$\text{Optimal State Projection: } \hat{s}_{k+1|k} = \mathbf{F}_k \hat{s}_{k|k-1} + \mathbf{K}_k\left[z_k - \mathbf{H}\hat{s}_k\right] \tag{9}$$

$$\text{Error Covariance Update: } \mathbf{P}_{k+1|k} = \mathbf{F}_k \mathbf{P}_{k|k-1}\mathbf{F}_k^T + E_{\psi_k}\left[\mathbf{G}\mathbf{Q}_k^o\mathbf{G}^T\right] - \mathbf{K}_k\left[\mathbf{H}\mathbf{P}_{k|k-1}\mathbf{H}^T + \mathbf{R}_k\right]\mathbf{K}_k^T \tag{10}$$

One can see that Eq's 8, 9, and 10 are very similar to the those used in the KF. However, the terms $E_{\psi_k}[\mathbf{G}]$ and $E_{\psi_k}\left[\mathbf{G}\mathbf{Q}_k^o\mathbf{G}^T\right]$ are conditional expectations, not known *a priori* as in the KF. Further, it is these two quantities that result in PLID's nonlinearities. Before the PLID equations can be implemented, a method of calculating $E_{\psi_k}[\mathbf{G}]$ and $E_{\psi_k}\left[\mathbf{G}\mathbf{Q}_k^o\mathbf{G}^T\right]$ must be obtained. This is a lengthy process, which is detailed in Hopkins *et al.*; we wish to now focus on the results of the on going experimental research. PLID has been coded into MATLAB on a 486 PC using Bierman's square root filter algorithm, which helps to insure that $\mathbf{P}_{k+1|k}$ remains positive definite in the presence of numerical round off. Although such algorithms add significantly to the number of computations per iteration (as much as 10x more), we are investigating model sizes that range up to 64 states. With such a large number of parameters to estimate, we were forced to use square root techniques.

3.0 RESULTS

3.1 Description of testbed

Conclusive determination of the value of an ID method can only be made after a hardware evaluation. Towards this end, we have fabricated, instrumented, and taken experimental transfer functions (TF's) of a 3-D truss structure. The graphic in Fig. 1 illustrates the testbed's important features.

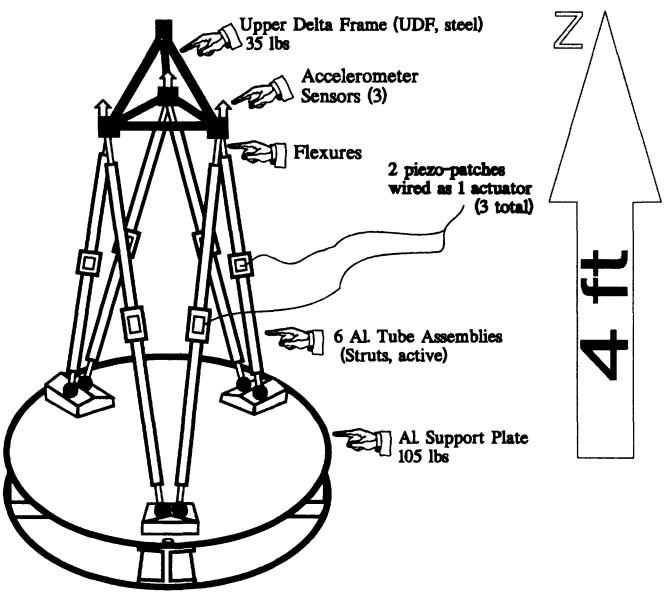

Fig. 1) Sketch of 3-D testbed

Total structural weight was measured at 140 lbs, with an overall height of 4-1/2 ft, including the support plate. The tubes and support plate were constructed out of aluminum, while the UDF was made from steel to increase its weight. This was done so that the vibrational modes of interest were below 200 Hz. We chose 200 Hz as the "soft" upper frequency limit

because of the computational limitations of the PC used for this study. It is interesting to note that the 1st rigid body vibrational resonance (or mode) of the UDF is approximately 136 Hz, as we shall see in Fig. 4. Considering that the UDF weighs 35 lbs, the support tube wall thickness is only 0.049", and that these struts are 3 ft long, one might expect that the 1st mode would be significantly lower than 136 Hz. Kinematic mounts, such as the one utilized in this structure, are quite stiff because all structural members are loaded purely axially.

3.2 Sensors

Notice the UDF in Fig. 1 has 3 accelerometers (manufactured by Wilcoxon Research, model 731-201) mounted vertically at the 3 corners (see Fig. 2). These are placed to provide observability to tip, tilt, and delta-z (piston) motions of the UDF. The accelerometer gain can be set at 10, 100, and 1000 V/*g*. We chose the 100 V/*g* sensitivity that can measure acceleration levels down to 0.05 milli-*g*'s, corresponding to a 5 mV electrical noise floor (limited by the 12-bit A/D converters). Weight of the sensor is ~0.067 lbs, or 30.5 grams.

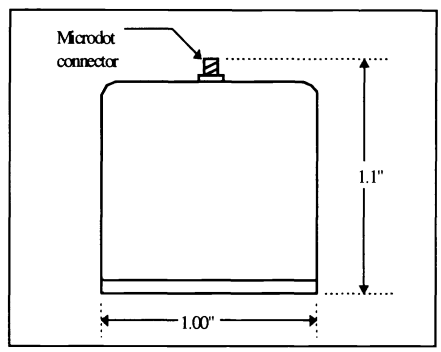

Fig. 2) Sketch of Wilcoxon 731-201 accelerometer

Using these sensors, measurements were taken of the undisturbed testbed to measure the ambient vibrations. Levels varying between 15 mV to 20 mV RMS were recorded. Thus, a typical noise level of 17.5 mV RMS was used to estimate the noise covariances. It is difficult to precisely pinpoint how each of the three noise sources (input, state, and output) contributed to this 17.5 mV RMS total noise signal. However, we had to make an "educated guess" in order for PLID to have a realistic representation of the sensor signal from which it will generate its parameter estimates.

Sensor noise was estimated to be approximately 5 mV. In part, this was motivated by the resolution of the 12-bit A/D converters used to digitized the sensor signal. The smallest signal that can be registered is 2.5 mV, and typically this bit is flipping, yielding 2*2.5 = 5 mV. Output measurements made of the actuator power amps with its inputs grounded showed that the actuators also contained approximately 5 mV of noise. Further, they too are driven by 12-bit D/A converters, which limits the resolution to 2.5 mV. One can consider this quantization error as noise, albeit not white. As we shall see, PLID is robust to such noise approximations. Subsequent study revealed that a 1V RMS actuator command (white noise) produced ~0.5 V RMS sensor signal. Based on this, we assumed that the 5 mV actuator noise could account for 2.5 mV of the observed total sensor noise (17.5 mV). This left 17.5 - 5 - 2.5 = 10 mV RMS of noise remaining, which was attributed to state noise. Sensor noise displayed little correlation between the 3 channels. Thus, it was assumed that the actuator, state, and sensor noise covariance matrices were diagonal. That is, the actuator noise was entered into MATLAB as $\mathbf{Q}_k$ = 0.005*eye(m,m), sensor noise was given by $\mathbf{R}_k$ = 0.005*eye(p,p), and the state noise entered as Σ_k = 0.010*eye(n,n).

3.3 Actuators

Actuation is provided by 0.02" x 1.00" x 2.00" piezo-ceramic wafers (manufactured by Vernitron[6], type PZT-5H) epoxied onto the flat section of an aluminum tube assembly (struts) using a cyanoacrylate instant epoxy (see Fig. 3).

Piezos on the two struts that connect to the same corner of the UDF are wired together such that when a voltage is applied, the associated UDF corner will translate bidirectionally along the Z-axis.

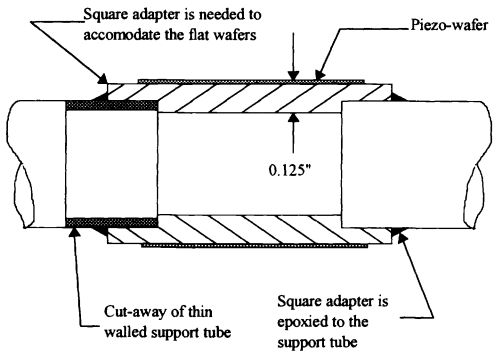

Fig. 3) Sketch of the mid-section of the support tube where that piezo-actuators are attached

Because of the thin wall of the aluminum support tubes (0.049"), the square adapter had to be epoxied, instead of welded to the tube. This resulted in a joint with higher than desired damping, and a slow time varying stiffness. Stiffness is also a function of temperature. Nonlinearities have been observed and are attributed to this joint. The result is a challenging testbed, which required several re-identification steps to account for time variations. Both the time variance and nonlinearities were not so severe as to cause PLID any difficulty, as we shall see.

When a voltage is applied, the piezo-wafers will elongate or contract depending on the voltage polarity. We can estimate the effectiveness of these actuators using knowledge of the piezo's electro-mechanical properties, and the geometry of the substructure. To do so rigorously is difficult because the piezo-properties are seldom known to better than 10%. This is one of the reasons system ID is so attractive, because all we need to do is size the actuator approximately to provide the desired actuation, and let the system ID algorithm provide, in effect, the calibration.

Actuator sizing was accomplished as follows. A full-scale sensor signal is 5 volts; with a sensitivity of 100 V/*g*, we have 0.05 *g*'s peak acceleration. The highest acceleration occurs at the highest frequency if the displacement is kept constant. Indeed, the actuators provide a constant displacement for a constant voltage. We do not wish to go into great detail of how piezo-ceramics are used and modeled; there are a great many excellent papers on the subject.[7,8] Briefly, the key parameter, in this case, is the "d_{31}" coefficient. It is defined as the strain generated along the wafer length divided by the electric field applied through the wafer thickness. The table below summarizes the important piezo properties:

Table 1) Piezo-ceramic properties for PZT-5H (± 20%)

Parameter	Value	Units	Description
d_{31}	1.1×10^{-8}	in./in. / V/in.	Charge constant
Ep	8.8×10^{6}	lbs / in.^{2}	Young's modulus
t	0.020	in.	Wafer thickness
l	2.00	in.	Wafer length
w	1.00	in.	Wafer width
C	24	nf	Bonded wafer capacitance
Max. Voltage	200	V	Break down limit

If we assume we have a perfect bond, we can greatly simplify our task. This allows us to simply ratio the stiffness of the square adapter to that of the piezo-ceramic. Below we derive the actuator output equation:

$$\text{Strain Output @ wafer:} \quad \varepsilon_1^{wafer} = d_{31} \cdot \frac{V_a}{t}, \tag{11}$$

where V_a = actuator voltage,

$$\text{Strain Output of actuator:} \quad \varepsilon_1^a = d_{31}\left(\frac{V_a}{t}\right)\left(\frac{Ep \cdot t}{E_{al} \cdot t_{sa}}\right), \tag{12}$$

where E_{al} = Young's modulus for the aluminum (10 x 10^6 psi), and t_{sa} = thickness of square adapter (0.125"); finally:

$$\text{Actuator Displacement output:} \quad \Delta L_1^a = d_{31}\left(\frac{l}{t}\right)\left(\frac{Ep \cdot t}{E_{al} \cdot t_{sa}}\right)Va, \tag{13}$$

The minimum number of wafers that can be epoxied to the square adapter is 2, one on either side as shown in Fig. 3 (to avoid bending the tube). Equation 13 must therefore be multiplied by 2. The only free parameter is the square adapter's thickness t_{sa}, because the wafers pre-dated this project, fixing all of its parameters (d_{31}, l, t, Ep). Sensor full-scale range must be taken into consideration to find t_{sa}. The equations below will determine t_{sa}, where ω is the operating frequency.

$$\text{Max. output displacement:} \quad \Delta L_1^a(\max) = \frac{g^{\max}\left(386 \ \frac{\text{in.}}{\text{sec}^2}\right)}{\omega^2}, \tag{14}$$

Solving for t_{sa}, we find:

$$\text{Square Adapter Thickness:} \quad t_{sa} = d_{31}\left(\frac{l}{t}\right)\left(\frac{Ep \cdot t \cdot \omega^2}{E_{al} \cdot g^{\max}\left(386 \ \frac{\text{in.}}{\text{sec}^2}\right)}\right)Va, \tag{15}$$

Finally, recall that $g^{\max}$ = 0.05 g's, ω = 200 Hz = 1256.6 rad/sec, and V_a(max) = 100 V. After substitution, t_{sa} is found to be ~0.16". Early on, we assumed that the bond was perfect. To allow for bond compliance, and to use a standard wall thickness, we decided to set t_{sa} = 0.125", as noted in Fig. 3.

Of course this analysis is very simplistic, especially considering that the actuator excitation will not be a pure sine wave at 200 Hz. Instead, filtered (or shaped) white noise with a bandwidth of 0 to 200 Hz will be used, which will generate significantly less acceleration because of the ω^2 term in Eq. 14's denominator. However, we have not included the amplification effect that a lightly damped structural resonance has. All we were after here is a "ball-park" actuator strength; we can adjust the power amp's gain if we need to account for simplifications made above.

Power amps were designed and built using the Apex PA-85A op-amps, which can provide up to 200 mA of output current, and 100 V peak. The D/A output signal is increased from ± 10 V to 100 V by the amp's 10x fixed gain. Attached to the nearly pure capacitive load of the piezos, these amps maintain a bandwidth of over 10 kHz. Thus, we have a means by which we can excite the testbed using the piezos and sense the resulting vibrations with the accelerometers, giving us the required input/output data.

In an attempt to limit the high-frequency gain of the system (motivated by the ω^2 actuator to sensor relationship), all 3 actuators were augmented by a one pole filter with a break frequency of 260 Hz. These poles, although known, were assumed to be part of the unknown plant. We did this to "fool" PLID to avoid an over emphasis on noisy high-frequency dynamics. We will discuss this further in the following sections. Two pole butterworth filters with a 1000 Hz break frequency provided aliasing protection.

3.4 Testbed characterization

Transfer functions were produced experimentally using a Hewlett Packard 3562A Dynamic Signal Analyzer (here forward referred to as the "HP") by random excitation in through the piezoelectric wafers and sensing with the

accelerometers. For every input/output pair a TF is generated, thus there are 3*3 = 9 such pairs. Figure 4 shows output #2/input #1, between 50 to 300 Hz. The first group of peaks seen near 60 Hz are the support tubes resonating. They are low in amplitude because the tubes are light relative to the UDF and the frequency is low, yielding a low acceleration. With each tube we have 2 modes, and 2 states per mode. Thus, 12 states would be needed to model these dynamics exactly. However, because these modes are about 40 dB below the dominant peaks, we would like to be able to use only a few states to model an average level.

The next resonance occurs at 136 Hz, corresponding to a rigid body mode of the UDF. Following this we have modes at 168, 186, and 212 Hz. These four modes are the ones of most interest to us because they fall within, or near, the bandwidth where disturbance vibrations exist (in our case, 10-200 Hz). However, we cannot completely ignore the dynamics between 212 and 400 Hz, because these modes are likely to be in the roll-off region of the closed loop controller. That is, in order to achieve some level of vibration attenuation, we must have significant controller gain in the frequency band of interest. Opposing this is our need to roll-off the compensator as fast as possible to avoid high-frequency instability. We must decide, at some point, on the frequency above which detailed knowledge is no longer required, otherwise our model will become too large to implement in a real-time controller, which is our goal (to be documented in the future).

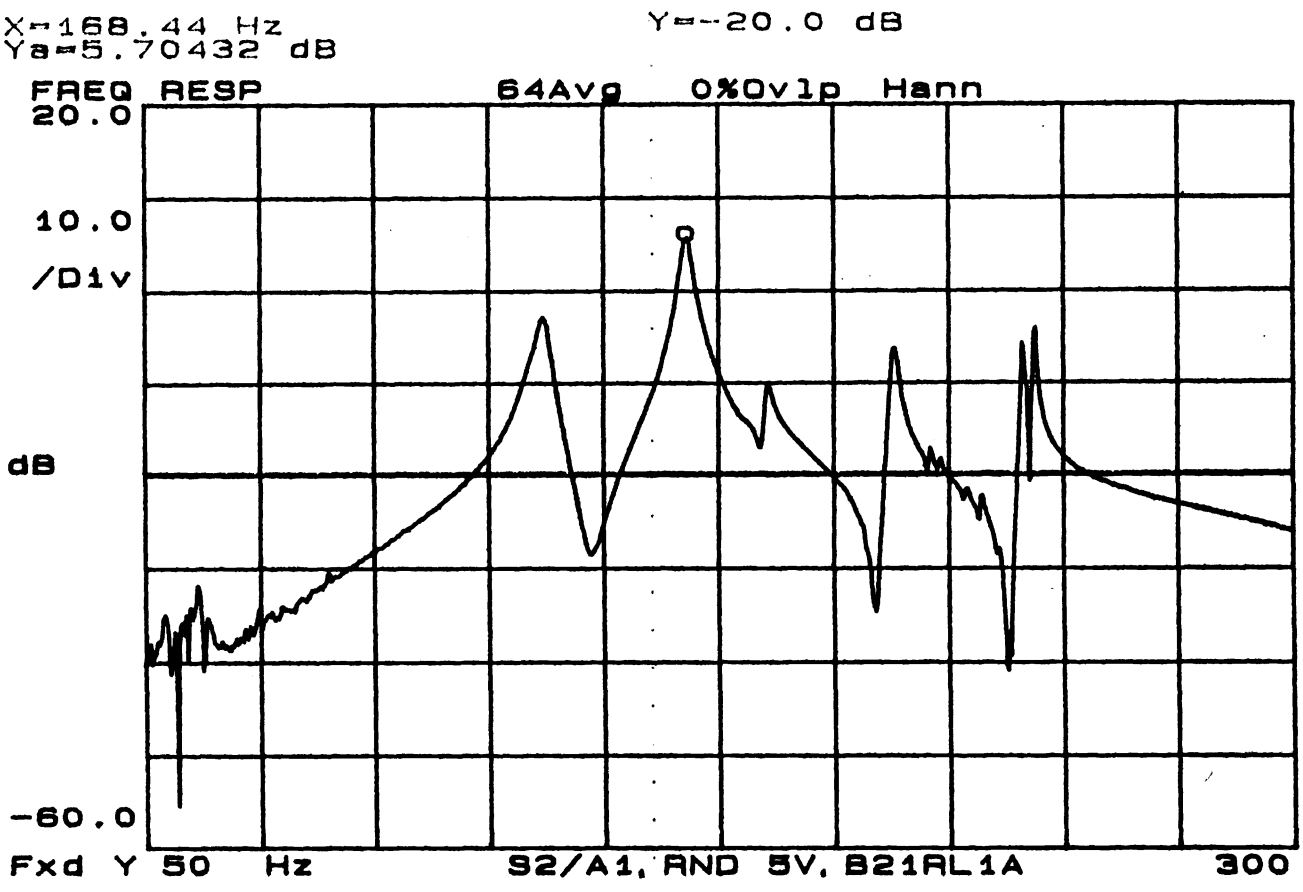

Fig. 4) TF generated by the HP 3562A using random excitation with 64 averages [sensor #2 / actuator #1]

The decision of what frequency to begin "truncating" the model depends on numerous factors. Two important ones are; (1) the performance level desired, and (2) the type of controller to be used. Our performance goal is modest; attenuate by 15 to 20 dB the dominant resonant peak levels below 200 Hz. The proposed controller is an LQG type augmented with high-frequency shaping filters (yet to be designed).[9,10] With such a controller, it should be possible to roll the loop transfer gain(s) off quickly, such that no resonance above 2*200 = 400 Hz will cause an instability. This may be wishful thinking, but this is what we have assumed for now.

It is possible to use the HP to create a model of the testbed. One way to accomplish this is by performing narrowband zooms at each resonance, curve fitting these zooms, and compiling all of the damping and natural frequency measurements in a large Laplace transfer function, or matrix of transfer functions in the MIMO case. Clearly this becomes an impractical method for large flexible structures. PLID needs only a few seconds of input/output data to generate a model (in this case). PLID can be used to create SISO or MIMO models, and makes no assumptions on the open loop plant stability, nor does it require the plant to be minimum phase.

3.5 Testbed data collection

To de-emphasize the high-frequency dynamics, it was necessary to roll-off the actuator input energy. This was done by passing the white actuator time series through a 6th order butterworth low-pass filter (see PSD in Fig. 5). PLID will recognize that the input has structure, which will not be included in the state space model. Thus, input frequency shaping is an effective way to reduce the model order. Model reduction done in this way will be "graceful" because PLID will not

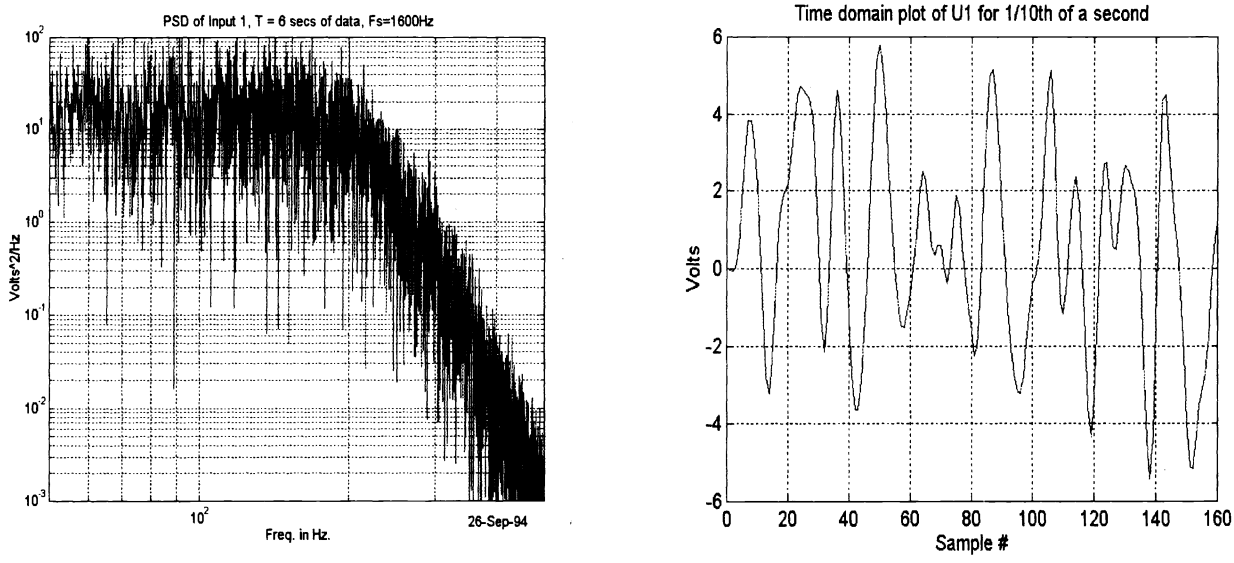

Fig. 5) PSD (left) and time domain (right) plot of the actuator signal

give as much attention to modes that are only weakly excited. Part of the reason is that in the setup for the solution of the optimal gain K_k we used the extended state error as the quantity to be minimized. Recall that the MIMO observable canonic form has the observations as states, thus directly wrapping the sensor error into the quantity to be minimized. The result is that high frequency modes not excited will not receive as much attention. Eventually, the 6 pole low-pass filter will reduce the actuation signal to well below both the actuator and sensor noise floor; PLID will not assign any poles above this frequency. With 6 poles, we reach this frequency around 600 Hz.

A sample rate of 1600 Hz was chosen based on the 200 Hz control bandwidth. It is high enough over 200 Hz to avoid sample rate effects, but not so high as to create a high correlation between samples. That is, we wish to set the sample rate as near to 2*600 Hz as possible to maintain a high information content in each sample. Doing this minimized the number of samples that PLID must be given to converge on the dynamics of interest.

Three independent signals are sent to each of the three actuators, while simultaneously sampling each of the three sensors. Simultaneity is important to avoid introducing artificial lag into the system. Both input and output are digitized by 12-bit zero order hold (ZOH) I/O cards (made by Intelligent Instrumentation) installed in a 486-66DX2 EISA (extended industry standard architecture) PC. Their boards were chosen because they allow the A/D and D/A to be synchronized.

Data collected are then copied from a memory buffer to the hard disk, and stored in ASCII single precision. Up to 13 seconds of data at a 1600 Hz sample rate can be taken this way with 3 channels.

3.6 Experimental results

3.6.1 MIMO results

The input/output data files are read in by MATLAB and stored in the work space. This is then fed to PLID one sample at a time. At every iteration, a plot of the absolute value of the maximum difference between the actual sensor voltage and the one-step ahead predicted sensor voltage is updated. We call this curve a "convergence plot", since our goal is to be able to reproduce or converge to the actual sensor signal. Every 50 iterations, a bode magnitude plot (or TF) of the estimated model, automatically annotated with frequency and peak level measurements from the HP, is provided. This is very useful for tracking PLID's progress.

To reduce the effects of noise, 10 data series, each 4 seconds long, are collected using exactly the same actuator input series. A linear system should return the same sensor data each time, differing only by the noise. Averaging these time series will decrease the effects of noise, as well as nonlinearities, as long as they are uncorrelated between time series. Peak noise levels were reduced from 40 mV to 20 mV with 10 averages. Noise reduction has a direct impact on the convergence plot as shown in Fig. 6. The plot on the left reaches a steady state level of ~30 mV, versus ~20 mV for the right plot.

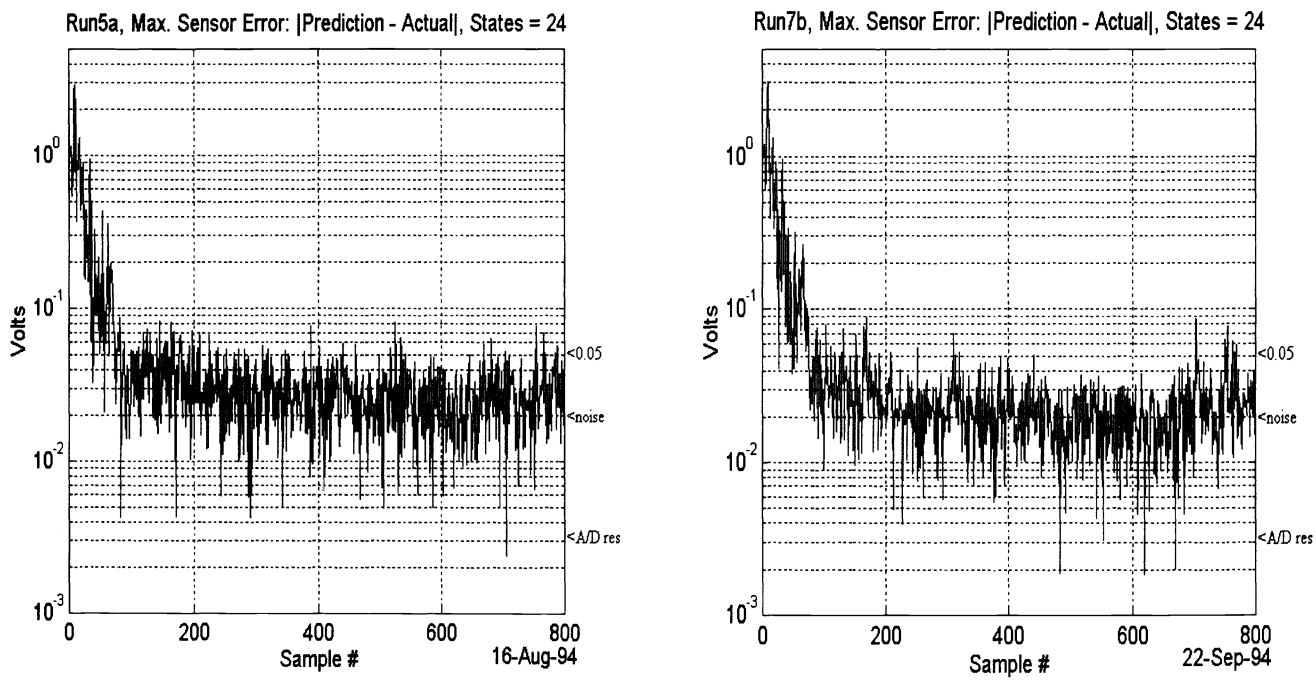

Fig. 6) Convergence plot without (left) and with (right) averaging

It also improves the match between the HP and PLID generated TF plot. We have annotated a TF plot generated in MATLAB with data taken by the HP for purposes of comparing experiment to theory. (Note: we apologize for not overlaying the HP and PLID plots directly. We were not able to get the HP data into the PC where we could plot the two together. Further, scanning the HP plots requires more RAM than we have available.)

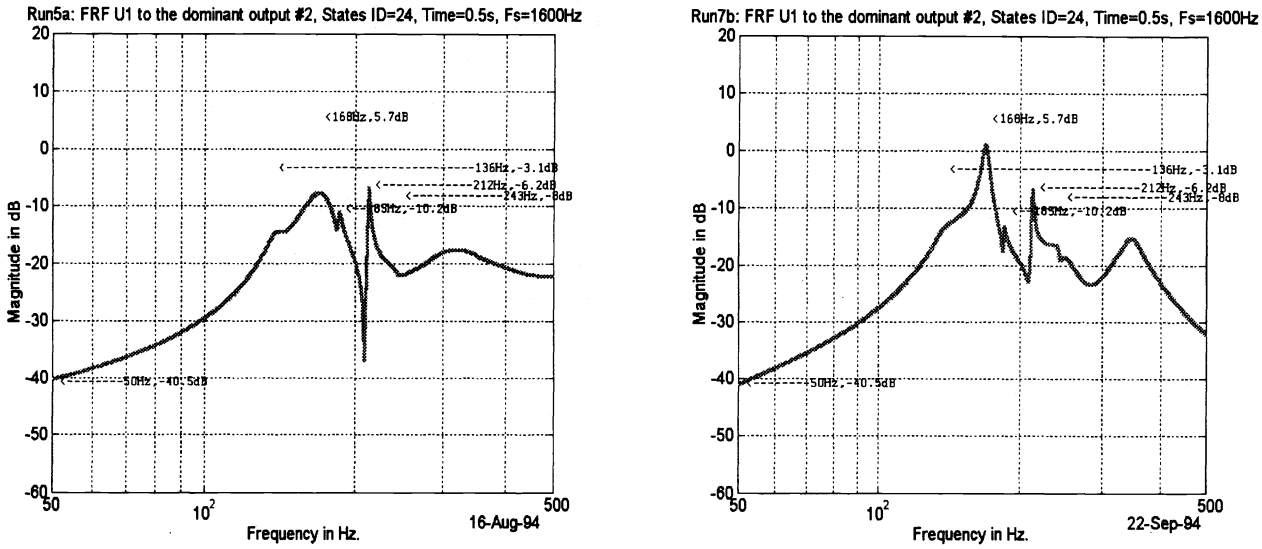

Fig. 7) TF plots using input #1 to output #2 without (left) and with (right) averaging

In the above plots, the MIMO version of PLID was used. That is, all three actuators and sensors were analyzed simultaneously. One can see from the right-hand plot in Fig. 7 that, even with averaging, we have not accurately converged to the correct dB level of the 136 Hz mode, but averaging clearly improves the performance. Many of the other modes are also not accurately captured. Sensor noise or algorithm limitations maybe the cause of this. Model size could also be to blame; it is very easy to check this hypothesis by increasing the model size, and re-generating the TF plot.

Unfortunately, when we ran a 36-state MIMO analysis, we ran out of RAM and virtual memory before the algorithm was done. However, we were able to try 27 states and 30 states, which show improvements as we increase the number of states. Figure 8 shows the 27 state (left) and 30 state TFs, both generated with 10 averages.

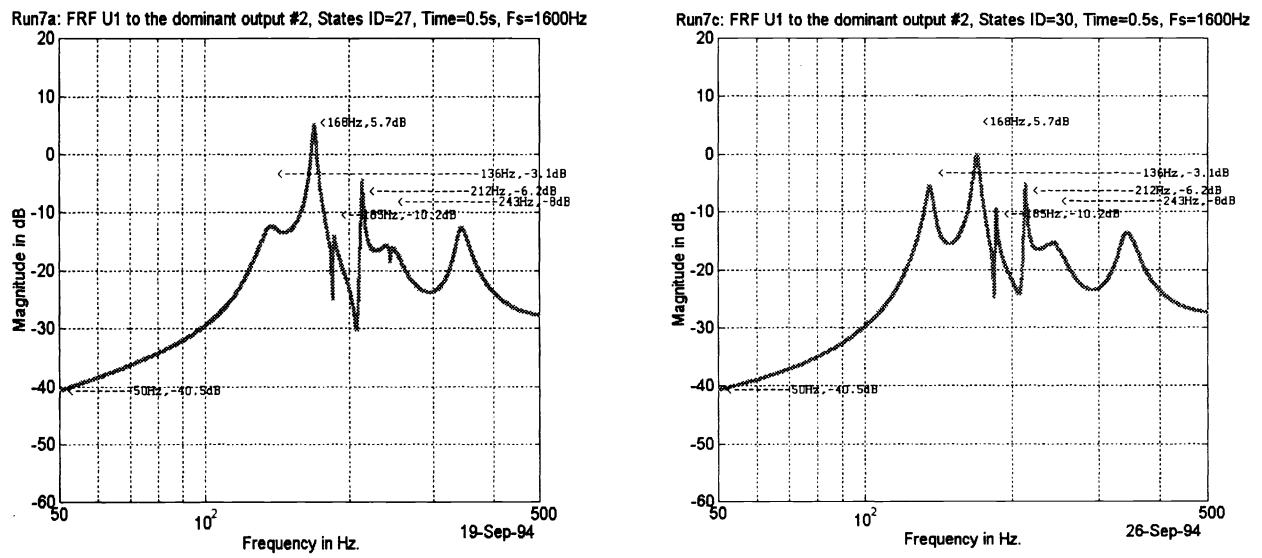

Fig. 8) MIMO TF plots using input #1 to sensor #2, 27 (left) and 30 states (right)

Predicted peaks that match the experimental peaks to within 3 dB are considered a match because of the time-varying nature of this plant. To keep the number of times that the experimental TFs had to be regenerated, we were forced to use data that was a month old. For this discussion, however, we are able to see that 30 states is, in general, the best match. However, the 168 Hz mode is significantly lower than measured. (Note: It was found later that this error occurred

because we had not let PLID run through enough samples. We'll discuss this in section 3.6.2). We cannot increase the states any more due to memory limitations, and increasing the number of samples given to PLID would result in an excessive run time. In order to go any further, a reformulation of the problem was needed. PLID was told to treat the problem as 3 separate SIMO systems, the results of which are given next.

3.6.2 SIMO results

The SIMO formulation has several advantages over the MIMO version. First, in this case, the execution time was cut in half when comparing a single SIMO run to the MIMO run. With the ever-dropping price of multi-CPU computers, comes the possibility to run each of the 3 SIMO models simultaneously on separate CPUs. Thus, the effective speed up is 2x. With even larger number of inputs and outputs, and more CPUs, the speed up could be much higher.

The second advantage follows directly from the first. Less computations means less computational error propagating through the simulation. All that remains to be done is to come up with an automated method of concatenating the 3 SIMO models into 1 MIMO model. We can perform this procedure "by hand", but this *ad hoc* concatenation requires detailed knowledge of the system and a certain amount of experience. We do believe, however, that automation is possible using only the information gathered by PLID. Work is continuing in this area.

Figure 9 shows the results of a 1500 sample run of SIMO PLID. The first 4 modes agree very well with the HP. At the 243 Hz mode a discrepancy still exists. A reasonable explanation for this can be seen from the convergence plot. The peak error is nearly always below the noise floor of the sensor. When this occurs, PLID will essentially assume it is done. Further, the 243 Hz mode is the 2nd smallest resonance and occurs after the 200 Hz 6 pole filter has begun to strongly roll-off. All of these factors, coupled with only 5 dB of error, suggests that the resulting sensor prediction errors will be small indeed.

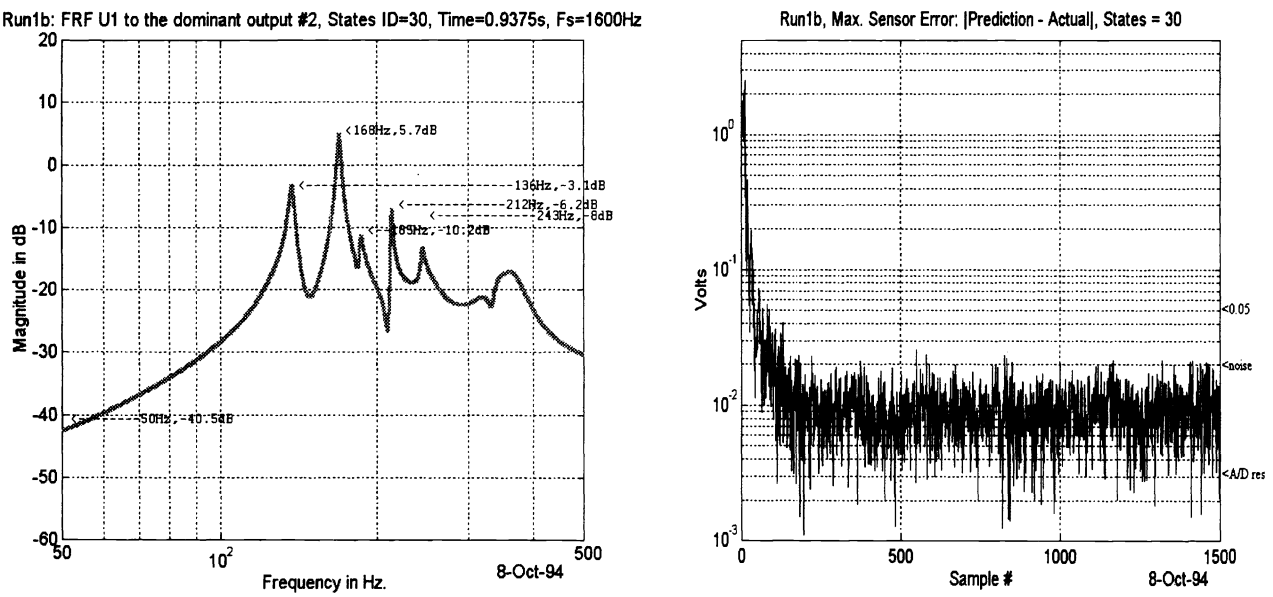

Fig. 9) SIMO plots using input #1 to sensor #2, TF (left) and convergence plot (right)

With the speedup realized by the SIMO models, we could explore still larger models, stepping through 35, 40, 45, 50, and 64 states. Again, RAM limited us to 64 states. These results are summarized by plotting the execution time (sec/iteration) versus the mean of the absolute value of the difference between the actual and PLID's one-step ahead predicted sensor voltage. Sensor error is averaged over the last 200 iterations of that particular run. Figure 10 shows the results obtained to date. This chart is useful for trading model accuracy with size, especially if you plan on using the model for real-time control.

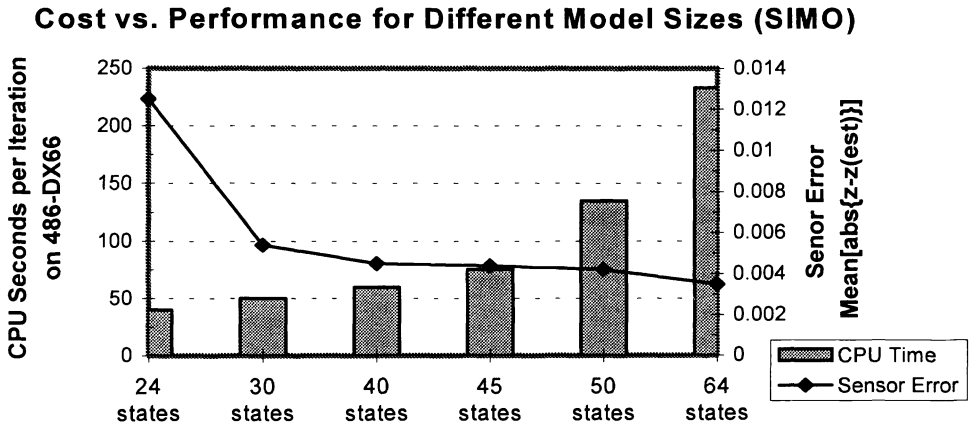

Fig. 10) SIMO performance plot, CPU cost vs model size

4.0 CONCLUSIONS

We have shown that PLID is a promising technique for identifying a state space model of a plant whose dynamics are unknown, and whose states, inputs, and outputs are all corrupted by noise. Results from the testbed are very encouraging, resulting in an "signal to residual error" ratio of greater than 200x (46 dB) using a reduced order model.

The one-step ahead predicted sensor output agrees with the actual output to within the peak noise levels of the accelerometers. Thus PLID must have optimally, or very nearly optimally, chosen the reduced order model to approximate the actual system, otherwise one would see a structured difference between the actual and predicted sensor output. The absence of such correlated error implies that the prediction is accurate to within the noise level of the system.

Future work will involve closing the loop on the testbed using an LQG controller, possibly augmented with Loop Transfer Recovery (LTR) techniques used to improve robustness. However, the purpose of the system ID work is to lessen, or entirely eliminate the need for LTR and to automate the controller design process. Typically a significant amount of "human intervention" is needed in the controller design. With a high-fidelity model and a well-defined bandwidth and performance goal, it is hoped that a batch adaptive controller can be realized for systems as complex as flexible structures. Most controller designs include gain and phase margins, which are conservative in order to avoid stability problems. Typically, with increased gain margin comes decreased performance. If the system can be periodically ID'd, the need for the larger gain margin goes away, improving performance.

5.0 REFERENCES

1. M. A. Hopkins, and H. F. VanLandingham, 1994, "Optimal Nonlinear Estimation of Linear Stochastic Systems", *ASME Journ. of Dyn. Syst., Meas., and Control*, Vol. 116, pp. 529-536, Sept. 1994.

2. R. G. Brown, and P. Y. C. Hwang, *Introduction to Random Signals and Applied Kalman Filtering*, John Wiley & Sons, Inc., New York, 1992

3. G. Salut, J. Aguilar-Martin, and S. Lefebvre, "New Results on Optimal Joint Parameter and State Estimation of Linear Stochastic Systems", *Transactions of the ASME*, 102, pp. 28-34, 1980.

4. G. J. Bierman, *Factorization Methods for Discrete Sequential Estimation*, Academic Press, Inc., New York, 1977.

5. T. Kailath, 1980, *Linear Systems*, Prentice-Hall, New Jersey, 1980.

6. Morgan Matroc Inc., Vernitron Division, "Guide to Modern Piezoelectric Ceramics", Manufacturer's Product Data Sheet, 232 Forbes Road, Bedford, Ohio, (216) 232-8600, undated.

7. E. F. Crawley and J. de Luis, "The use of piezoelectric actuators as elements of intelligent structures," *AIAA Journ.*, Vol. 25, No. 10, AIAA Paper 86-0878, Oct. 1987.

8. E. F. Crawley and E. F. Anderson, "Detailed models of piezoceramic action of beams," *Journ. of Intell. Mater. Syst. and Struct.*, Vol. 1, Jan. 1990.

9. A. Grace, A. J. Laub, J. N. Little, and C. Thompson, *Control System Toolbox, User's Guide*, Massachusetts: The MathWorks, Inc., 1990.

10. H. Kwakernaak, *Linear Optimal Control Systems*, New York: Wiley-Interscience, a division of John Wiley & Sons, Inc., 1972.